Article

A ligand insertion mechanism for cooperative NH_3 capture in metal–organic frameworks

https://doi.org/10.1038/s41586-022-05409-2

Received: 12 January 2022

Accepted: 4 October 2022

Published online: 11 January 2023

Check for updates

Benjamin E. R. Snyder[1,4], Ari B. Turkiewicz[1], Hiroyasu Furukawa[1,2], Maria V. Paley[1,2], Ever O. Velasquez[2,3], Matthew N. Dods[1,3] & Jeffrey R. Long[1,2,3] ✉

Ammonia is a critical chemical in agriculture and industry that is produced on a massive scale via the Haber–Bosch process[1]. The environmental impact of this process, which uses methane as a fuel and feedstock for hydrogen, has motivated the need for more sustainable ammonia production[2–5]. However, many strategies that use renewable hydrogen are not compatible with existing methods for ammonia separation[6–9]. Given their high surface areas and structural and chemical versatility, metal–organic frameworks (MOFs) hold promise for ammonia separations, but most MOFs bind ammonia irreversibly or degrade on exposure to this corrosive gas[10,11]. Here we report a tunable three-dimensional framework that reversibly binds ammonia by cooperative insertion into its metal–carboxylate bonds to form a dense, one-dimensional coordination polymer. This unusual adsorption mechanism provides considerable intrinsic thermal management[12], and, at high pressures and temperatures, cooperative ammonia uptake gives rise to large working capacities. The threshold pressure for ammonia adsorption can further be tuned by almost five orders of magnitude through simple synthetic modifications, pointing to a broader strategy for the development of energy-efficient ammonia adsorbents.

The development of alternative methods for ammonia (NH_3) separation that could replace refrigeration condensation has been identified as a critical step in the realization of more efficient, sustainable and decentralized NH_3 production[6–9]. Metal halides dispersed in solid supports have garnered interest for this purpose, as they can operate effectively at relatively low pressures and high temperatures and exhibit NH_3 capacities that exceed those of activated carbons and zeolites[8,9]. Porous, tunable metal–organic frameworks (MOFs) have also been studied for NH_3 capture, largely in the context of storage[13] and health and safety[10]. However, examples that are stable to NH_3—particularly under cyclical exposure—remain scarce[10,11]. Frameworks featuring robust metal–linker bonds and coordinatively unsaturated metal sites capable of strongly binding NH_3 offer some advantages[10], although the large enthalpies associated with NH_3 binding at open metal sites and typical Langmuir-type adsorption behaviour are not ideal for practical applications.

In recent years, several metal–carboxylate frameworks featuring coordinatively saturated metal sites have been reported to have large regenerable NH_3 capacities[14–17] that, in many cases, greatly exceed the predicted capacities based on a physisorptive pore-filling adsorption mechanism[14–16]. On the basis of spectroscopic and/or gravimetric analysis, it has been proposed that NH_3 uptake in these materials occurs through chemisorption following disruption of the metal–carboxylate bonds. In the case of Cu(bdc) (bdc^{2-} = 1,4-benzenedicarboxylate), the formation of a one-dimensional coordination polymer Cu(bdc)$(NH_3)_2$ was proposed on the basis of powder X-ray diffraction data[15], although this structure was not reconciled with measured NH_3 uptake in the material. While harnessing reversible adsorbate insertion in MOFs is an attractive strategy for the design of robust NH_3 adsorbents, this phenomenon has yet to be conclusively demonstrated and controlled. Here we present a detailed study of NH_3 uptake in the crystalline, air-stable framework Cu(cyhdc) ($cyhdc^{2-}$ = *trans*-1,4-cyclohexanedicarboxylate)[18,19], which features coordinatively saturated copper(II) sites. On the basis of gas adsorption as well as single-crystal and powder X-ray diffraction data, NH_3 adsorption in this material triggers reversible, temperature- and pressure-dependent cooperative phase transitions, and as a result, Cu(cyhdc) is highly selective for uptake of NH_3 over nitrogen (N_2) and hydrogen (H_2). The threshold pressure for NH_3 insertion can also be tuned by nearly five orders of magnitude through judicious choice of metal and linker within the Cu(cyhdc) structure type. This work provides evidence for a guest-induced structural transformation driving selective NH_3 capture in a MOF, with relevance to the design of phase-change adsorbents for NH_3 capture and separations.

The framework Cu(cyhdc)[18,19] features one-dimensional chains of dicopper paddlewheel units connected by ditopic *trans*-1,4-cyclohexanedicarboxylate linkers to form a three-dimensional structure with rhombic channels along the *c* axis (Fig. 1a and Supplementary Fig. 1). Each metal centre features four equatorial carboxylate oxygens and a fifth axial carboxylate oxygen from a linker of a neighbouring paddlewheel unit (Fig. 1b). NH_3 adsorption data collected for microcrystalline Cu(cyhdc) at 298 K revealed stepwise uptake of

[1]Department of Chemistry, University of California, Berkeley, Berkeley, CA, USA. [2]Materials Sciences Division, Lawrence Berkeley National Laboratory, Berkeley, CA, USA. [3]Department of Chemical and Biomolecular Engineering, University of California, Berkeley, Berkeley, CA, USA. [4]Present address: Department of Chemistry, University of Illinois at Urbana-Champaign, Urbana, IL, USA. ✉e-mail: jrlong@berkeley.edu

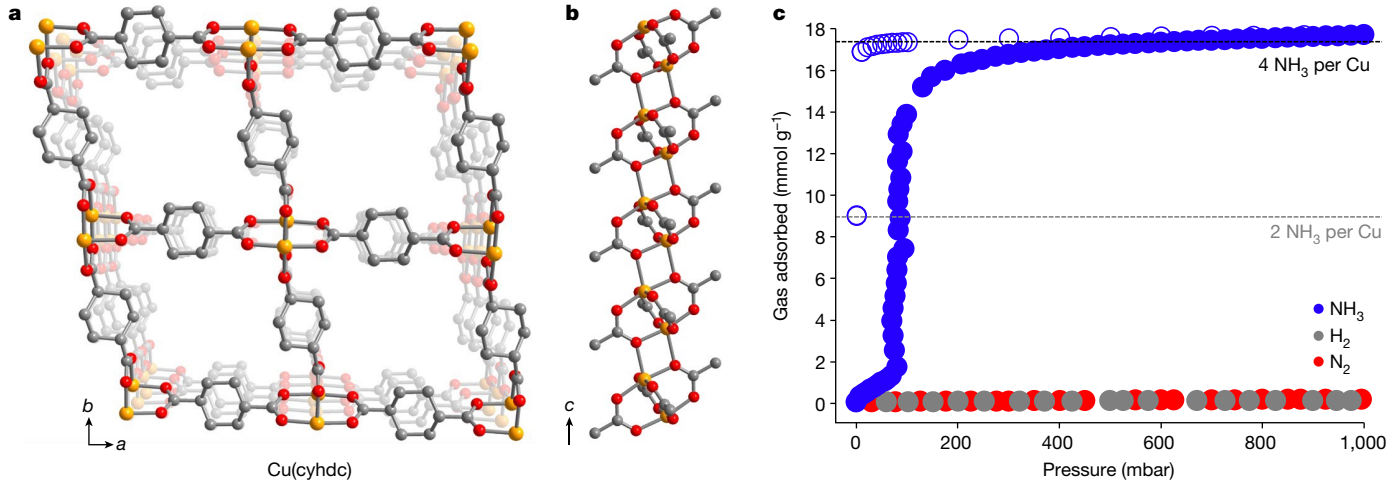

Fig. 1 | Structure of Cu(cyhdc) and NH_3 uptake. a, Illustration of the structure of the framework Cu(cyhdc) showing the rhombic channels with vertices formed by Cu–carboxylate paddlewheel units[18]. Orange, red, and grey spheres represent Cu, O and C atoms, respectively; H atoms are omitted for clarity. **b**, Side view of the one-dimensional copper paddlewheel chain motif that defines the pore vertices. **c**, NH_3 adsorption and desorption isotherms (filled and empty blue circles, respectively) obtained at 298 K for Cu(cyhdc) (no additional NH_3 uptake is seen at pressures up to 6 bar; see Supplementary Fig. 2 and further discussion in the main text). N_2 and H_2 adsorption isotherms are shown in red and grey for comparison. The grey and black dashed lines indicate NH_3 capacities associated with adsorption of two and four equivalents of NH_3 per Cu site, respectively.

approximately 16 mmol g^{-1} at a pressure of about 80 mbar (Fig. 1c). The uptake plateaus above 100 mbar, giving rise to a relatively flat post-step region and a saturation capacity of 17.5 mmol g^{-1} at 1 bar, corresponding to adsorption of 4 equivalents of NH_3 per copper site. Notably, Cu(cyhdc) adsorbs minimal N_2 and H_2 under the same conditions (Fig. 1c), and its gravimetric NH_3 capacity is among the highest reported so far for porous solids (20–24 mmol g^{-1} at 298 K and 1 bar)[10,20]. The stepped adsorption characterized here for Cu(cyhdc) is fairly unique among NH_3 adsorbents, and is indicative of a phase change and/or cooperative transition following NH_3 uptake[8,12,21,22]. Although step-shaped NH_3 uptake has been characterized in select systems, including non-porous metal halides, these materials are proposed to adsorb NH_3 through pore-filling or intercalation mechanisms typically associated with slow uptake kinetics and/or low capacities[15,23–25].

When exposed to NH_3, Cu(cyhdc) changes colour from green to blue, indicating a change in the coordination environment of the Cu(II) centres. Powder X-ray diffraction analysis of Cu(cyhdc) dosed with 1 bar NH_3 revealed that this blue solid is microcrystalline and forms a different phase than the MOF (Supplementary Fig. 3). X-ray diffraction analysis of single crystals of this phase (see Methods and Supplementary Fig. 4) revealed that it is the non-porous, one-dimensional coordination polymer $Cu(NH_3)_4$(cyhdc) (Fig. 2a,b). The structure of $Cu(NH_3)_4$(cyhdc) consists of symmetry-equivalent Cu(II) centres coordinated by four equatorial NH_3 ligands (Cu–N bond lengths of 2.014(2) Å and 2.057(2) Å) and two axial bridging *trans*-1,4-cyclohexanedicarboxylate linkers bound by a single oxygen atom (d_{Cu-O} = 2.468(2) Å). Each NH_3 engages in hydrogen bonding interactions with secondary-sphere oxygen atoms (ranging from approximately 2.0 Å to 2.2 Å), and each carboxylate oxygen interacts with nearby NH_3 ligands, resulting in a stabilizing network of moderately short hydrogen bonds. On the basis of literature data correlating hydrogen bond lengths and enthalpies[26] and density functional theory (DFT) calculations (see Methods), this network affords an estimated stabilization energy of at least 40 kJ mol^{-1} NH_3, which, together with strong NH_3 binding, probably contributes substantially to the driving force for NH_3 uptake. Preliminary analysis further suggests that the transition is associated with rapid adsorption kinetics and minimal material expansion, both desirable characteristics for solid NH_3 sorbents (see Methods)[27,28].

Hysteresis is apparent upon isothermal NH_3 desorption from $Cu(NH_3)_4$(cyhdc) (Fig. 1c), and only half of the NH_3 is desorbed at 1 mbar, suggesting the formation of an intermediate structure with 2 NH_3 per Cu. Indeed, after desorption, the solid changes colour from the characteristic blue of $Cu(NH_3)_4$(cyhdc) to purple. Powder X-ray diffraction analysis revealed that the purple solid is a new phase that forms from $Cu(NH_3)_4$(cyhdc) (Supplementary Fig. 5). X-ray diffraction analysis of single crystals of this phase (see Methods for details) revealed it to be the one-dimensional solid $Cu(NH_3)_2$(cyhdc), featuring square planar Cu(II) centres coordinated by two *trans* NH_3 and two *trans* carboxylate ligands bound by a single oxygen atom (Fig. 2c and

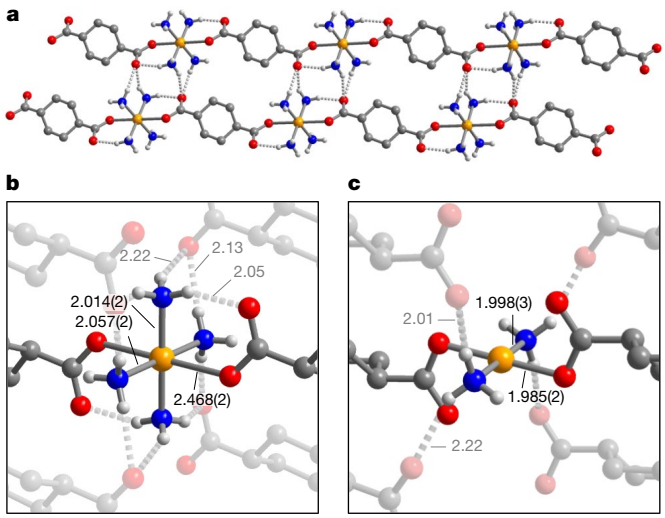

Fig. 2 | Single-crystal X-ray diffraction structure of $Cu(NH_3)_4$(cyhdc) and the local Cu environment in $Cu(NH_3)_2$(cyhdc). a, Illustration of the structure of $Cu(NH_3)_4$(cyhdc) as obtained from single-crystal X-ray diffraction analysis, showing hydrogen bonding interactions between adjacent polymer chains. **b**, Local Cu environment in $Cu(NH_3)_4$(cyhdc). **c**, Representative view of the coordination environment of the Cu sites in $Cu(NH_3)_2$(cyhdc) (see Supplementary Fig. 6 for an extended structure view). Select Cu–linker and hydrogen bond distances are given in Å. Hydrogen bonds are indicated with dashed lines. No errors are reported on hydrogen bond distances, as H atoms were refined using a riding model. Orange, red, blue, grey and white spheres represent Cu, O, N, C and H atoms, respectively; H atoms of the $cyhdc^{2-}$ linkers are omitted for clarity.

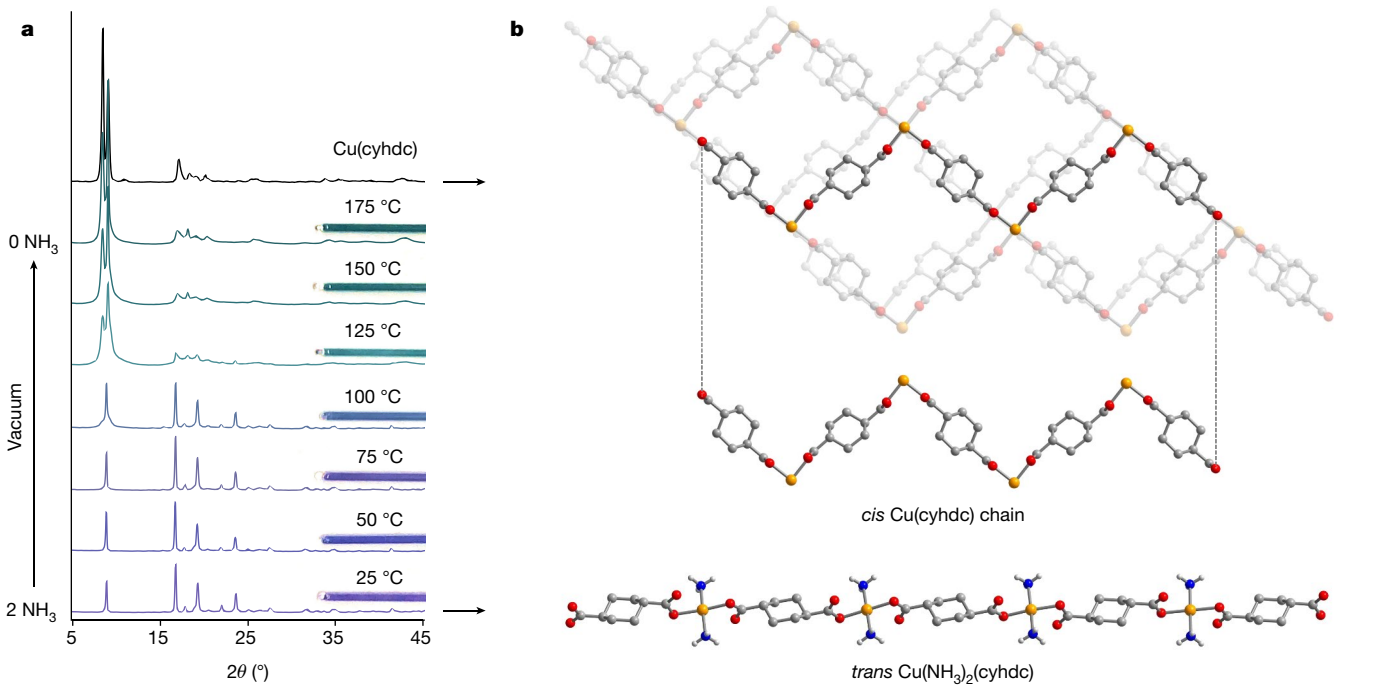

Fig. 3 | Ammonia desorption from $Cu(NH_3)_2(cyhdc)$. a, Powder X-ray diffraction data (2θ is the diffraction angle) collected while heating pristine $Cu(NH_3)_2(cyhdc)$ (purple trace; see Methods) under dynamic vacuum to regenerate Cu(cyhdc) (green trace). Images of the material (in capillaries) are included above the corresponding powder patterns, showing the colour changes that correlate with NH_3 desorption. The diffraction pattern for pristine Cu(cyhdc) is shown for comparison (black trace). **b**, Illustration of the relationship between the structures of $Cu(NH_3)_2(cyhdc)$ (bottom) and Cu(cyhdc) (top) as discussed in the text. Orange, red, blue, grey and white spheres represent Cu, O, N, C and H atoms, respectively; H atoms of the $cyhdc^{2-}$ linkers are omitted for clarity.

Supplementary Figs. 6–8). Powder X-ray diffraction analysis confirmed that it is possible to regenerate porous Cu(cyhdc) from this phase (Fig. 3a and Supplementary Fig. 9), and it is also possible to regenerate Cu(cyhdc) directly from $Cu(NH_3)_4(cyhdc)$ (Supplementary Fig. 10).

This polymeric phase with 2 NH_3 per Cu is isostructural to that reported to form upon NH_3 uptake in Cu(bdc)[14], although the reported NH_3 uptake of this material (about 17 mmol g^{-1} at 298 K and 1 bar, but with a type I isotherm profile) corresponds closely to adsorption of 4 NH_3 at each Cu site. This discrepancy was attributed to an adventitious binding site that could not be resolved crystallographically, although our own preliminary characterization of NH_3 uptake in Cu(bdc) suggests that the phase with 4 NH_3 bound per Cu is amorphous (Supplementary Fig. 8). At present, is unclear why Cu(bdc) becomes amorphous under NH_3 exposure whereas Cu(cyhdc) yields a crystalline product.

Thermogravimetric analysis (TGA) of $Cu(NH_3)_4(cyhdc)$ revealed that NH_3 desorption under a flow of N_2 occurs in two steps at 50 °C and 125 °C, each associated with loss of two NH_3 (Supplementary Fig. 11), and TGA cycling experiments revealed that NH_3 adsorption in Cu(cyhdc) and stepwise desorption via $Cu(NH_3)_2(cyhdc)$ is robust over at least six adsorption–desorption cycles with no apparent loss in NH_3 capacity (about 30 wt% or 17.4 mmol g^{-1}; Supplementary Figs. 12 and 13). A closer examination of the structures of Cu(cyhdc) and $Cu(NH_3)_2(cyhdc)$ provides insight into the stability of this transformation. The $Cu(NH_3)_2(cyhdc)$ structure features *trans* Cu(cyhdc) chains (Fig. 3b, bottom), whereas *cis* Cu(cyhdc) chains (Fig. 3b, middle) can be considered as a basis for the structure of Cu(cyhdc) (Fig. 3b, top). Bringing together *cis* Cu(cyhdc) chains in the same plane generates two-dimensional square grids with Cu paddlewheel nodes, which can be linked by dangling carboxylate oxygen atoms from adjacent grids to form the three-dimensional framework (Supplementary Fig. 14). Thus, the transformation from $Cu(NH_3)_2(cyhdc)$ to Cu(cyhdc) can in principle be accomplished without cleaving a fundamental component of both structures—the Cu(cyhdc) chains. We are currently investigating the molecular-level mechanism of this interconversion.

Heats of adsorption for NH_3 binding at framework open metal sites typically range from −50 kJ mol^{-1} to more than −100 kJ mol^{-1} (refs. [20,29,30]). Such highly exothermic adsorption would substantially limit the performance of an adsorbent in an adiabatic separation process, or require additional energy and infrastructure to efficiently remove waste heat. However, the phase change that occurs upon NH_3 adsorption in Cu(cyhdc) could be sufficiently endothermic to offset a high heat of adsorption[12,31,32]. To investigate this possibility, we collected NH_3 adsorption isotherms for Cu(cyhdc) at additional temperatures of 273 K, 323 K and 348 K over a pressure range of 0 to 1 bar (Fig. 4a). At 273 K, stepped NH_3 uptake occurs with an onset pressure of about 22 mbar. The material saturates at 1 bar with a capacity of 18.7 mmol g^{-1}, reflecting the direct conversion of Cu(cyhdc) to $Cu(NH_3)_4(cyhdc)$. At 323 K, there are two adsorption steps at 130 mbar and 630 mbar, each corresponding to uptake of approximately 2 NH_3 per Cu, indicating stepwise conversion of Cu(cyhdc) to $Cu(NH_3)_2(cyhdc)$ to $Cu(NH_3)_4(cyhdc)$. At 348 K, a single step occurs at 260 mbar. The uptake plateaus at 10.2 mmol g^{-1} at 1 bar, corresponding to the adsorption of approximately 2 NH_3 per Cu.

From fits to isotherm data collected at 273 K and 298 K (see Methods and Supplementary Fig. 15), we calculated an isosteric heat of adsorption of −31 ± 3 kJ mol^{-1} NH_3 associated with the transformation of Cu(cyhdc) to $Cu(NH_3)_4(cyhdc)$ (Fig. 4b, black circles), whereas fits to the first step in the 323 K and 348 K data afforded an isosteric heat of adsorption of −24 ± 3 kJ mol^{-1}, corresponding to the conversion of Cu(cyhdc) to $Cu(NH_3)_2(cyhdc)$ (Fig. 4b, grey circles). We also extrapolated an isosteric heat of adsorption of −39 ± 4 kJ mol^{-1} NH_3 associated

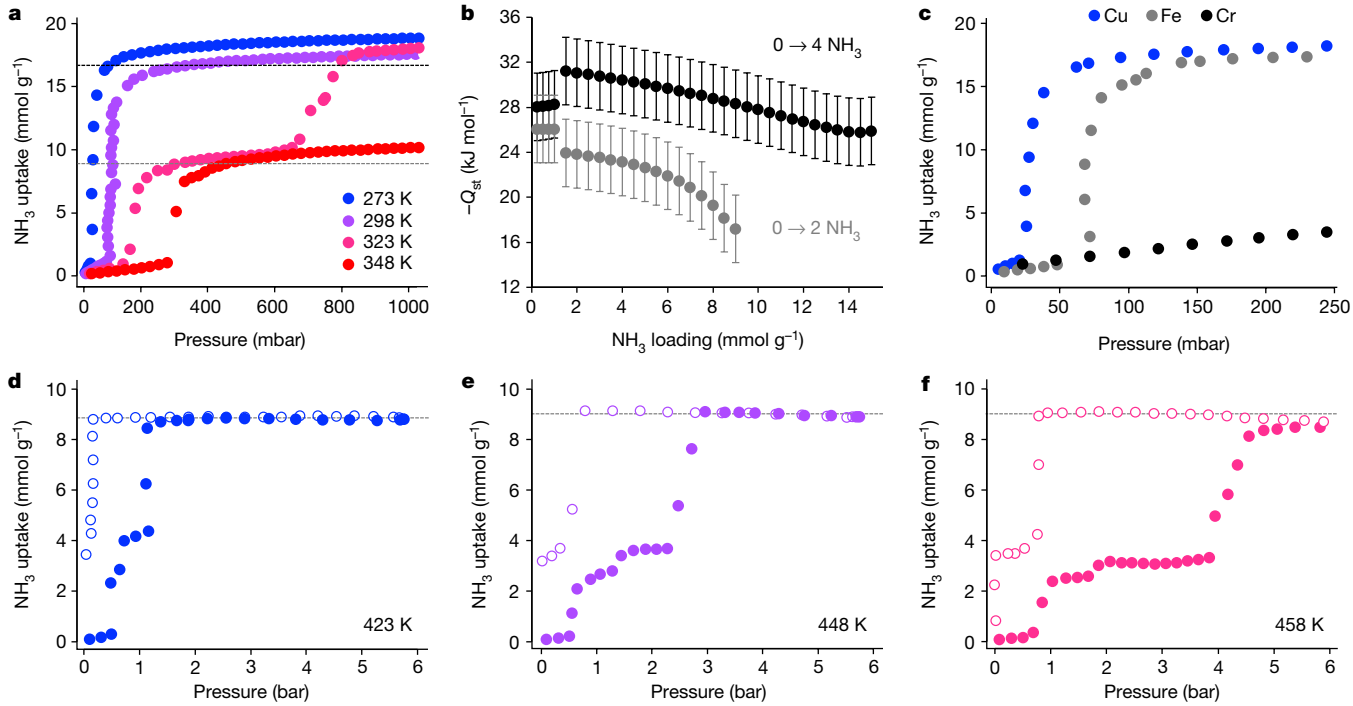

Fig. 4 | Temperature dependence of NH_3 adsorption in Cu(cyhdc) and impact of metal and linker variations on NH_3 uptake in M(dicarboxylate) frameworks. a, NH_3 adsorption isotherms collected for Cu(cyhdc) at various temperatures, revealing the temperature-dependent nature of the cooperative framework-to-chain solid phase change. The dashed grey and black lines correspond to predicted capacities associated with 2 NH_3 per Cu and 4 NH_3 per Cu, respectively. **b**, Variation of the isosteric heat of NH_3 adsorption with increasing loading. The isosteric heats calculated from fits to the 273 K and 298 K isotherm data (black circles) reflect the direct conversion of Cu(cyhdc) to $Cu(NH_3)_4$(cyhdc), whereas values calculated from fits to the 323 K and 348 K isotherm data from 0 to 500 mbar (grey circles) reflect the conversion of Cu(cyhdc) to $Cu(NH_3)_2$(cyhdc) (see Supplementary Fig. 15 and Methods for detail on these fits and definition of the associated error bars, which reflect uncertainty in the sample temperature and equilibration pressure). **c**, NH_3 adsorption data obtained at 273 K for microcrystalline Cu(cyhdc), Fe(cyhdc) and Cr(cyhdc). **d**–**f**, High-pressure (0–6 bar) NH_3 adsorption (filled circles) and desorption (empty circles) data collected for Cu(cyhdc) at 423 K (**d**), 448 K (**e**) and 458 K (**f**). The dashed lines indicate uptake corresponding to 2 NH_3 per Cu centre. Slight jumps in the NH_3 uptake observed between 1 bar and 2 bar are measurement artefacts; see Methods for details.

with the conversion of $Cu(NH_3)_2$(cyhdc) into $Cu(NH_3)_4$(cyhdc) at higher temperatures. In all, these low isosteric heats reflect the extent to which exothermic Cu–NH_3 bond formation is offset by phase changes involving endothermic Cu–O bond cleavage. Similarly, exothermic Cu–O bond formation during the transition from $Cu(NH_3)_4$(cyhdc) to Cu(cyhdc) probably facilitates regeneration at a lower temperature (125 °C) than is typically required to regenerate MOFs that adsorb NH_3 in the absence of a phase change (200 °C to 280 °C)[20,29,30].

We next investigated NH_3 adsorption in Cu(cyhdc) at higher temperatures (373 K, 423 K, 448 K and 458 K) and NH_3 pressures (0 to 6 bar) more relevant to proposed alternative methods for renewable NH_3 synthesis[9]. These challenging conditions are rarely explored for NH_3 adsorption in MOFs[33,34]. At 373 K, the NH_3 adsorption profile features two steps indicative of cooperative gas adsorption, each corresponding to uptake of approximately 2 NH_3 per Cu as observed at 323 K and pressures up to 1 bar (Fig. 4a), and the uptake plateaus at 16.8 mmol g^{-1} above 4.5 bar (Supplementary Fig. 2). At 423 K, 448 K and 458 K, NH_3 uptake is also associated with two adsorption steps, each corresponding to about 1 NH_3 per Cu (Fig. 4d–f). There is also some temperature dependence in the uptake in the plateau region after the first step (4.2 mmol g^{-1} at 423 K versus 3.0 mmol g^{-1} at 458 K). Maximum uptakes ranging from 8.2 mmol g^{-1} to 8.6 mmol g^{-1} were achieved at 423 K, 448 K and 458 K at pressures of 1.2 bar, 3.0 bar and 5.0 bar, respectively, suggesting the formation of a species with 2 NH_3 bound per Cu. These adsorption phenomena are the subject of ongoing investigation in our laboratory, although they support that cooperative NH_3 insertion also occurs in Cu(cyhdc) at higher temperatures and pressures. Of note, uptake of N_2 and H_2 is negligible at high temperature and pressures up to 6 bar (Supplementary Fig. 16).

Substantial hysteresis was observed upon desorption at each temperature, probably reflecting structural transitions that occur upon NH_3 desorption. At low pressure, the desorption isotherms plateau at an uptake of about 1 NH_3 per Cu, possibly owing to the formation of a $Cu(NH_3)$(cyhdc) phase. At 423 K and 448 K, this final equivalent of NH_3 remains bound at the lowest pressures (10 mbar), whereas at 458 K it is possible to desorb nearly all NH_3. Preliminary analysis of NH_3 desorption from Cu(cyhdc) following dosing at 6 bar and high temperatures revealed as-of-yet-unidentified crystalline products, suggesting more complex desorption behaviour than at lower pressures and temperatures, although the material appears to be regenerable (slight decomposition is evident after prolonged exposure at 6 bar and 458 K; see Methods). An estimated working capacity of 5.4 mmol g^{-1} can be achieved with a modest pressure swing (between 1.2 bar and 0.05 bar at 423 K), temperature swing (between 373 K and 458 K at 750 mbar) or pressure–temperature swing (between 1.2 bar at 423 K and 0.75 bar at 458 K). Under these conditions, Cu(cyhdc) outperforms the top solid sorbents studied for NH_3 capture, including select MOFs[33,34] and supported metal halides[23,27,35,36].

We sought to explore the versatility of this adsorbent platform and synthesized Fe(cyhdc) and Cr(cyhdc) – two crystalline, porous frameworks that are isostructural to Cu(cyhdc) (see Methods and Supplementary Figs. 17–20). At 273 K, Fe(cyhdc) exhibits stepped NH_3 adsorption corresponding to 4 NH_3 per iron atom, with an onset pressure of 70 mbar (compared with 20 mbar for Cu(cyhdc); Fig. 4c). Powder X-ray diffraction analysis of Fe(cyhdc) dosed with 1 bar NH_3 at

298 K suggests the formation of a one-dimensional structure akin to that of $Cu(NH_3)_4$(cyhdc) (Supplementary Fig. 17). Although Cr(cyhdc) shows only low NH_3 uptake at 298 K and 1 bar (Supplementary Fig. 21), high-pressure adsorption data revealed stepped uptake of about 4 NH_3 per chromium atom above 4 bar (Supplementary Fig. 22). The relative NH_3 affinities of Fe(cyhdc) and Cu(cyhdc) are consistent with the Irving–Williams series[37,38], whereas the much lower NH_3 affinity of Cr(cyhdc) probably reflects an additional driving force required to cleave the metal–metal quadruple bond within each Cr paddlewheel node. Frameworks with more labile Cu–carboxylate bonds are expected to adsorb NH_3 with even lower step pressures than Cu(cyhdc). To test this hypothesis, we synthesized Cu(bpdc) (where $bpdc^{2-}$ is 4,4′-biphenyldicarboxylate) and Cu(tfbdc) (where $tfbdc^{2-}$ is 2,3,5,6-tetrafluoro-1,4-benzenedicarboxylate) (Supplementary Figs. 18b and 23–25), which are isoreticular to Cu(cyhdc) but feature weaker carboxylate donors. As expected, the NH_3 adsorption step shifts to lower pressures upon moving from Cu(cyhdc) to Cu(bpdc) to Cu(tfbdc) (Supplementary Fig. 26). In fact, the Cu–carboxylate bonds of Cu(tfbdc) are sufficiently weak to enable cooperative adsorption of water (Supplementary Figs. 24, 27 and 28).

In summary, we have shown that NH_3 insertion into the Cu–carboxylate bonds of Cu(cyhdc) drives a robust, reversible cooperative phase change at low pressures, which enables rapid, high-capacity NH_3 uptake with intrinsic thermal management. Preliminary analysis indicates that Cu(cyhdc) shows cooperative NH_3 uptake at even higher pressures and temperatures relevant to sustainable methods for NH_3 synthesis[7–9]. More broadly, the foregoing results represent an important conceptual advance for the design of cooperative adsorbents for low-energy storage and separation applications involving coordinating gas molecules.

Online content

Any methods, additional references, Nature Portfolio reporting summaries, source data, extended data, supplementary information, acknowledgements, peer review information; details of author contributions and competing interests; and statements of data and code availability are available at https://doi.org/10.1038/s41586-022-05409-2.

1. Qing, G. et al. Recent advances and challenges of electrocatalytic N_2 reduction to ammonia. *Chem. Rev.* **120**, 5437–5516 (2020).
2. Guo, J. & Chen, P. Catalyst: NH_3 as an energy carrier. *Chem* **3**, 709–712 (2017).
3. Ye, T.-N. et al. Vacancy-enabled N_2 activation for ammonia synthesis on an Ni-loaded catalyst. *Nature* **583**, 391–395 (2020).
4. Li, K. et al. Enhancement of lithium-mediated ammonia synthesis by addition of oxygen. *Science* **374**, 1593–1597 (2021).
5. Suryanto, B. H. R. et al. Nitrogen reduction to ammonia at high efficiency and rates based on a phosphonium proton shuttle. *Science* **372**, 1187–1191 (2021).
6. Soloveichik, G. Electrochemical synthesis of ammonia as a potential alternative to the Haber–Bosch process. *Nat. Catal.* **2**, 377–380 (2019).
7. Smith, C., Hill, A. K. & Torrente-Murciano, L. Current and future role of Haber–Bosch ammonia in a carbon-free energy landscape. *Energy Environ. Sci.* **13**, 331–344 (2020).
8. Malmali, M. et al. Better absorbents for ammonia separation. *ACS Sustain. Chem. Eng.* **6**, 6536–6546 (2018).
9. Smith, C., McCormick, A. V. & Cussler, E. L. Optimizing the conditions for ammonia production using absorption. *ACS Sustain. Chem. Eng.* **7**, 4019–4029 (2019).
10. Rieth, A. J., Wright, A. M. & Dincă, M. Kinetic stability of metal–organic frameworks for corrosive and coordinating gas capture. *Nat. Rev. Mater.* **4**, 708–725 (2019).
11. Kajiwara, T. et al. A systematic study on the stability of porous coordination polymers against ammonia. *Chem. Eur. J.* **20**, 15611–15617 (2014).
12. Mason, J. A. et al. Methane storage in flexible metal–organic frameworks with intrinsic thermal management. *Nature* **527**, 357–361 (2015).
13. Godfrey, H. G. W. et al. Ammonia storage by reversible host–guest site exchange in a robust metal–organic framework. *Angew. Chem. Int. Ed.* **57**, 14778–14781 (2018).
14. Chen, Y. et al. Removal of ammonia emissions via reversible structural transformation in M(BDC) (M = Cu, Zn, Cd) metal–organic frameworks. *Environ. Sci. Technol.* **54**, 3636–3642 (2020).
15. Chen, Y. et al. Environmentally friendly synthesis of flexible MOFs $M(NA)_2$ (M = Zn, Co, Cu, Cd) with large and regenerable ammonia capacity. *J. Mater. Chem. A* **6**, 9922–9929 (2018).
16. Chen, Y., Li, L., Li, J., Ouyang, K. & Yang, J. Ammonia capture and flexible transformation of M-2 (INA)(M = Cu, Co, Ni, Cd) series materials. *J. Hazard. Mater.* **306**, 340–347 (2016).
17. Lyu, P. et al. Ammonia capture via an unconventional reversible guest-induced metal-linker bond dynamics in a highly stable metal–organic framework. *Chem. Mater.* **33**, 6186–6192 (2021).
18. Kumagai, H. et al. Metal–organic frameworks from copper dimers with *cis*- and *trans*-1,4-cyclohexanedicarboxylate and *cis*,*cis*-1,3,5-cyclohexanetricarboxylate. *Inorg. Chem.* **46**, 5949–5956 (2007).
19. Seki, K., Takamizawa, S. & Mori, W. Characterization of microporous copper(II) dicarboxylates (fumarate, terephthalate, and *trans*-1,4-cyclohexanedicarboxylate) by gas adsorption. *Chem. Lett.* **30**, 122–123 (2001).
20. Kim, D. W. et al. High ammonia uptake of a metal–organic framework adsorbent in a wide pressure range. *Angew. Chemie Int. Ed.* **59**, 22531–22536 (2020).
21. McDonald, T. M. et al. Cooperative insertion of CO_2 in diamine-appended metal-organic frameworks. *Nature* **519**, 303–308 (2015).
22. Reed, D. A. et al. A spin transition mechanism for cooperative adsorption in metal–organic frameworks. *Nature* **550**, 96–100 (2017).
23. Liu, C. Y. & Aika, K. Ammonia absorption on alkaline earth halides as ammonia separation and storage procedure. *Bull. Chem. Soc. Jpn* **77**, 123–131 (2004).
24. Kang, D. W. et al. A hydrogen-bonded organic framework (HOF) with type IV NH_3 adsorption behavior. *Angew. Chem. Int. Ed.* **131**, 16298–16301 (2019).
25. Chen, Y. et al. Antenna-protected metal–organic squares for water/ammonia uptake with excellent stability and regenerability. *ACS Sustain. Chem. Eng.* **5**, 5082–5089 (2017).
26. Steiner, T. The hydrogen bond in the solid state. *Angew. Chem. Int. Ed.* **41**, 48–76 (2002).
27. Wang, L., Chen, L., Wang, H. L. & Liao, D. L. The adsorption refrigeration characteristics of alkaline-earth metal chlorides and its composite adsorbents. *Renew. Energy* **34**, 1016–1023 (2009).
28. Wang, L. W., Wang, R. Z., Lu, Z. S., Chen, C. J. & Wu, J. Y. Comparison of the adsorption performance of compound adsorbent in a refrigeration cycle with and without mass recovery. *Chem. Eng. Sci.* **61**, 3761–3770 (2006).
29. Rieth, A. J., Tulchinsky, Y. & Dincă, M. High and reversible ammonia uptake in mesoporous azolate metal–organic frameworks with open Mn, Co, and Ni sites. *J. Am. Chem. Soc.* **138**, 9401–9404 (2016).
30. Katz, M. J. et al. High volumetric uptake of ammonia using Cu-MOF-74/Cu-CPO-27. *Dalt. Trans.* **45**, 4150–4153 (2016).
31. Hiraide, S., Tanaka, H., Ishikawa, N. & Miyahara, M. T. Intrinsic thermal management capabilities of flexible metal–organic frameworks for carbon dioxide separation and capture. *ACS Appl. Mater. Interfaces* **9**, 41066–41077 (2017).
32. Feldmann, W. K., Esterhuysen, C. & Barbour, L. J. Pressure-gradient sorption calorimetry of flexible porous materials: implications for intrinsic thermal management. *ChemSusChem* **13**, 5220–5223 (2020).
33. An, G. et al. Metal–organic frameworks for ammonia-based thermal energy storage. *Small* **17**, 2102689 (2021).
34. Liu, Z. et al. The potential use of metal–organic framework/ammonia working pairs in adsorption chillers. *J. Mater. Chem. A* **9**, 6188–6195 (2021).
35. Kale, M. J. et al. Optimizing ammonia separation via reactive absorption for sustainable ammonia synthesis. *ACS Appl. Energy Mater.* **3**, 2576–2584 (2020).
36. Hrtus, D. J., Nowrin, F. H., Lomas, A., Fotsa, Y. & Malmali, M. Achieving+ 95% ammonia purity by optimizing the absorption and desorption conditions of supported metal halides. *ACS Sustain. Chem. Eng.* **10**, 204–212 (2021).
37. Irving, H. & Williams, R. J. P. The stability of transition-metal complexes. *J. Chem. Soc.* 3192–3210 (1953).
38. Paoletti, P. Formation of metal complexes with ethylenediamine: a critical survey of equilibrium constants, enthalpy and entropy values. *Pure Appl. Chem.* **56**, 491–522 (1984).

Methods

General considerations

All reagents were purchased from commercial vendors and used as received. Ultrahigh-purity-grade (99.999%) helium, N_2 and H_2, and anhydrous NH_3 were used for all gas adsorption measurements. All Cu-containing frameworks were prepared under ambient conditions using as-received solvents. Cr(cyhdc) and Fe(cyhdc) were prepared under an inert N_2 atmosphere in a glovebox, using solvents that were degassed and dried over 3 Å molecular sieves before use. All DFT calculations were performed using Gaussian 16 revision A03[39].

Synthesis of Cu(cyhdc)

The framework Cu(cyhdc) was prepared using a modification of the procedure reported in ref. [18]. A 250 ml bottle was charged with $Cu(NO_3)_2{\cdot}2.5H_2O$ (2.326 g, 0.01000 mol), *trans*-1, 4-cyclohexanedicarboxylic acid (1.722 g, 0.01000 mol) and 100 ml *N*,*N*′-dimethylformamide. The blue solution was heated for 16 h in an oven at 90 °C. The resulting green–blue precipitate was isolated by filtration and rinsed three times with 25 ml aliquots of fresh *N*,*N*′-dimethylformamide. The precipitate was then rinsed three times with 25 ml aliquots of methanol, soaked in 100 ml fresh methanol for 24 h (two times) and then stored under 100 ml fresh methanol in a tightly sealed jar. The framework was activated by heating at 150 °C under vacuum for 18 h to 24 h. No colour change was observed upon activation. This procedure yields approximately 2 g of activated material and can be readily scaled up by a factor of at least 2.5. Advantageously, Cu(cyhdc) is made from inexpensive starting materials (H_2cyhdc is commercially available for around US$600 per kg) and is stable in the presence of water (H_2O) vapour and O_2 (Supplementary Fig. 37), allowing for facile handling under ambient conditions.

Preparation and handling of $Cu(NH_3)_4$(cyhdc) prepared from Cu(cyhdc) via dosing with NH_3 gas

In a typical preparation, an evacuated glass sample tube containing activated Cu(cyhdc) (up to 100 mg) was dosed with 1 bar NH_3 on a Micromeritics 3Flex gas adsorption analyser. A contact time of 15 min is generally sufficient for complete conversion, although 30 min is ideal (see 'Kinetics of NH_3 adsorption in Cu(cyhdc) and volume changes upon NH_3 uptake' below). $Cu(NH_3)_4$(cyhdc) prepared in this way is very sensitive. Exposure to atmospheric moisture results in a purple-coloured powder with a powder diffraction pattern that is distinct from $Cu(NH_3)_2$(cyhdc) (Supplementary Fig. 29, left). We were also unexpectedly able to structurally characterize this phase as the one-dimensional coordination polymer $Cu(NH_3)_2(H_2O)$(cyhdc), in which each Cu centre binds two equivalents of NH_3 and one equivalent of H_2O (Supplementary Fig. 29, right). This conversion is mostly complete after 4 min if the powder is exposed on a flat surface. However, if the sample is exposed in a walled vessel such as a 20 ml vial, the conversion appears to be slower. We find that samples held in 20 ml vials or TGA pans can generally be handled for 30–60 s in air before degrading. However, powder X-ray diffraction analysis is a facile method for evaluating sample purity, and the blue-to-purple colour change associated with NH_3 desorption/water adsorption is also distinctive.

Preparation of single crystals of $Cu(NH_3)_4$(cyhdc)

Approximately 20 mg Cu(cyhdc) was placed in a 20 ml vial. A 2.0 M solution of NH_3 in methanol was added until the framework was observed to be almost completely dissolved, resulting in a blue saturated solution. Crystals of $Cu(NH_3)_4$(cyhdc) suitable for single-crystal X-ray diffraction were grown by vapour diffusion: 1 ml of the saturated solution was added to an open 1.8 ml vial, which was then placed in a closed 20 ml vial containing 3 ml tetrahydrofuran. After standing for one to two days, brilliant blue needles formed. Methanol and *N*,*N*′-dimethylformamide are also effective anti-solvents in this scheme. Unlike microcrystalline $Cu(NH_3)_4$(cyhdc) prepared by dosing Cu(cyhdc) with gaseous NH_3, single crystals of $Cu(NH_3)_4$(cyhdc) prepared in this way are relatively stable, with gradual spontaneous loss of NH_3 leading to crystal degradation over the course of hours (not minutes). In an attempted synthesis using an NH_3/methanol solution that had absorbed atmospheric moisture during prolonged storage, we formed a one-dimensional polymer in which each Cu centre is coordinated by two NH_3 ligands and one H_2O ligand (Supplementary Fig. 29 and Supplementary Table 1). This is the same phase that forms when $Cu(NH_3)_4$(cyhdc) is exposed to ambient atmosphere (see 'Preparation and handling of $Cu(NH_3)_4$(cyhdc) prepared from Cu(cyhdc) via dosing with NH_3 gas' above). Therefore, although rigorously dry solvents are not required to grow single crystals of $Cu(NH_3)_4$(cyhdc), it is advisable to use only new or recently opened solutions of NH_3/methanol.

Characterization of $Cu(NH_3)_2$(cyhdc) formed by desorption of NH_3 from $Cu(NH_3)_4$(cyhdc)

Approximately 100 mg of microcrystalline $Cu(NH_3)_4$(cyhdc) prepared by dosing Cu(cyhdc) with gaseous NH_3 was held under dynamic vacuum (80 mbar) on a Schlenk line at room temperature. The solid was characterized by ex situ powder X-ray diffraction analysis (Cu Kα) at regular intervals for 18 h (Supplementary Fig. 5). After 18 h, the powder X-ray diffraction pattern of the evacuated material correlated well with that predicted from the single-crystal X-ray diffraction structure of $Cu(NH_3)_2$(cyhdc) (Supplementary Fig. 6). The powder X-ray diffraction data in Supplementary Fig. 5 indicate that this transformation was mostly complete after 30 min.

Direct synthesis of $Cu(NH_3)_2$(cyhdc)

Microcrystals. Approximately 50 mg Cu(cyhdc) was placed in a 20 ml vial and suspended in 18 ml methanol. A 1.5 ml solution of 2.0-M NH_3 solution in methanol was added in 0.25 ml increments over the course of two days. A colour change to blue began within 30 min after the second 0.25 ml aliquot (0.5 ml total). The powder began to turn purple within 30 min of adding the fourth 0.25 ml aliquot. The supernatant remained colourless throughout. The resulting free-flowing bright purple powder was isolated by filtration, rinsed with three 10 ml aliquots of fresh methanol, and dried on a Schlenk line for 16 h at room temperature.

Single crystals. Approximately 20 mg Cu(cyhdc) was placed in a 20 ml vial. A 2.0 M solution of NH_3 in methanol was added until the framework was observed to be almost completely dissolved, resulting in a blue saturated solution. One millilitre of this saturated solution was added to an open 1.8 ml vial, which was then sealed inside a 20 ml vial containing 5 ml of a 1:1 (v:v) solution of methanol and ethanol. Small purple crystals formed after sitting for two to three days. We found that the growth of high-quality crystals of this material is strongly dependent on the choice of anti-solvent. In particular, although $Cu(NH_3)_4$(cyhdc) can be crystallized using tetrahydrofuran, methanol or *N*,*N*-dimethylformamide as the anti-solvent, these solvents were not suitable for crystallization of $Cu(NH_3)_2$(cyhdc), and only the 1:1 methanol/ethanol solution was found to be effective.

Desorption of NH_3 from $Cu(NH_3)_2$(cyhdc) to form Cu(cyhdc)

Approximately 50 mg of microcrystalline $Cu(NH_3)_2$(cyhdc) prepared as described in 'Direct synthesis of $Cu(NH_3)_2$(cyhdc)' was placed in a 20 ml vial and heated under dynamic vacuum (80 mbar) on a Schlenk line for 24 h at each of the following temperatures in succession: 50 °C, 75 °C, 100 °C, 125 °C, 150 °C and 175 °C. At the end of each 24 h period, a sample of the solid was analysed by powder X-ray diffraction (Cu Kα). The resulting data are plotted in Fig. 3a.

Synthesis of Cu(bdc)

The framework Cu(bdc) was prepared using a modification of the procedure reported in ref. [18]. A 250 ml bottle was charged with

$Cu(NO_3)_2{\cdot}2.5H_2O$ (2.326 g, 0.01000 mol), 1,4-benzenedicarboxylic acid (1.661 g, 0.01000 mol) and 100 ml *N*,*N*′-dimethylformamide. The bottle was sealed, and the blue solution was heated for 16 h in an oven at 90 °C. The resulting pale blue precipitate was isolated by filtration and rinsed three times with 25 ml aliquots of fresh *N*,*N*′-dimethylformamide. The precipitate was then rinsed three times with 25 ml aliquots of methanol, soaked in 100 ml fresh methanol for 24 h (two times), and then stored under 100 ml fresh methanol in a tightly sealed jar. The material changes colour to a darker shade of blue upon activation and slowly degrades in the presence of atmospheric moisture.

Synthesis of Cr(cyhdc)

In a dry N_2 glovebox, a 20 ml vial was charged with anhydrous chromium(II) chloride (0.200 g, 0.00163 mol), *trans*-1, 4-cyclohexanedicarboxylic acid (0.172 g, 0.00100 mol), 8 ml *N*,*N*′-dimethylformamide and 1 ml methanol. The blue solution was heated for 18 h on a hot plate at 120 °C, resulting in a fine orange precipitate that was collected by filtration. The solid was rinsed three times with 10 ml aliquots of methanol, then soaked in 10 ml fresh methanol for 24 h (two times). No colour change was observed upon activation. This material is very sensitive to O_2 and will change colour from salmon orange to brown in a matter of seconds upon exposure to pure O_2 or air. The material exposed to pure O_2 remains crystalline. However, it degrades rapidly upon exposure to ambient air, changing colour from brown to green in minutes with loss of crystallinity.

Synthesis of Fe(cyhdc)

In a dry N_2 glovebox, a 20 ml vial was charged with anhydrous iron(II) chloride (0.200 g, 0.00158 mol), *trans*-1,4-cyclohexanedicarboxylic (0.172 g, 0.00100 mol), 8 ml *N*,*N*′-dimethylformamide and 1 ml methanol. The faint yellow solution was heated for 18 h on a hot plate at 120 °C, resulting in a grey precipitate that was collected by filtration. The solid was rinsed three times with 10 ml aliquots of methanol, then soaked in 10 ml fresh methanol for 24 h (two times). No colour change was observed upon activation. This material is slightly sensitive to O_2, and upon exposure to pure O_2 or ambient atmosphere it slowly changes colour—from light grey to pale yellow—over the course of 24 h.

Synthesis of Cu(bpdc)

A 250 ml bottle was charged with $Cu(NO_3)_2{\cdot}2.5H_2O$ (2.326 g, 0.01000 mol), biphenyl-4,4′-dicarboxylic acid (1.211 g, 0.005000 mol) and 100 ml *N*,*N*′-dimethylformamide. The blue solution was heated for 16 h in an oven at 90 °C. The resulting teal precipitate was isolated by filtration, and rinsed three times with 25 ml fresh *N*,*N*′-dimethylformamide. The precipitate was then rinsed three times with 25 ml aliquots of methanol, soaked in 100 ml fresh methanol for 24 h (two times) and then stored under 100 ml fresh methanol in a tightly sealed jar. The material changes colour subtly to a darker blue upon activation and slowly degrades in the presence of atmospheric moisture.

Synthesis of Cu(tfbdc)

A 250 ml bottle was charged with $Cu(NO_3)_2{\cdot}2.5H_2O$ (2.326 g, 0.01000 mol), tetrafluoroterephthalic acid (2.381 g, 0.01000 mol) and 100 ml ethanol. The resulting blue solution was heated for 16 h in an oven at 60 °C. The resulting pale blue precipitate was isolated by filtration, and rinsed three times with 25 ml fresh ethanol. Finally, the material was soaked in 100 ml fresh ethanol for 24 h (two times) and stored under 100 ml fresh ethanol. The resulting solid was isolated by vacuum filtration and heated to 120 °C under dynamic vacuum for 18 h to obtain activated Cu(tfbdc). The activated material is a dark blue–green colour and is highly sensitive to moisture. This material is also more temperature sensitive than the other Cu frameworks studied here: activation at 150 °C was noted to cause some browning of the material.

Preparation of single crystals of $Cu(H_2O)_2$(tfbdc)

Deionized water (10 ml) was added directly to a sample of about 100 mg freshly activated Cu(tfbdc), resulting in a saturated solution. Five millilitres of this saturated solution was filtered through a cotton pad to remove solid Cu(tfbdc) and allowed to stand in an open 20 ml vial on the bench. After evaporation of about 4 ml of this solution, blue plates of $Cu(H_2O)_2$(tfbdc) had formed alongside colourless needles, which were identified as a different phase based on powder X-ray diffraction analysis.

Gas adsorption measurements

Gas adsorption isotherms were collected using a Micromeritics ASAP2420 or Micromeritics 3Flex gas adsorption analyser. MOF samples of approximately 40–60 mg were transferred to pre-weighed analysis tubes, which were then capped with TranSeals. Unless specified otherwise, samples were activated by heating to 150 °C with a ramp rate of 0.2 °C min^{-1} under dynamic vacuum until an outgas rate of less than 2 μbar min^{-1} was achieved (typically 18 h). The evacuated analysis tube containing the activated sample was then reweighed to determine the sample mass. For isotherms collected at 298 K, 323 K and 348 K, samples were immersed in a Syltherm bath heated with a water recirculator. Isotherms collected at 273 K were measured using an ice-water bath. N_2 isotherms collected at 77 K were measured using a liquid-nitrogen bath. Langmuir surface areas were calculated from 77 K N_2 adsorption data (from points in the 50–250 mbar region) using Micromeritics software. Oil-free vacuum pumps and oil-free pressure regulators were used for all measurements to prevent contamination of the samples during the evacuation process or of the feed gases during the isotherm measurements.

Isosteric heats of NH_3 adsorption

Isosteric heats of NH_3 adsorption (Q_{st}) were calculated according to the method outlined in ref. [22]. The isosteric heat for the direct conversion of Cu(cyhdc) to $Cu(NH_3)_4$(cyhdc) was calculated from the 273 K and 298 K isotherms (Fig. 4a and Supplementary Fig. 15). The isosteric heat for the conversion of Cu(cyhdc) to $Cu(NH_3)_2$(cyhdc) was calculated from the 323 K and 348 K isothermal data collected below 500 mbar (that is, covering the first adsorption step; Fig. 4a). In both cases, the isosteric heats determined for NH_3 adsorption below 1 mmol g^{-1} reflect pore filling. Error bars of ±3 kJ mol^{-1} associated with the calculated values allow for ±1 K error in measurement temperature and ±5% error in the equilibrium pressure. This is probably an overestimate of the measurement error.

Interestingly, the calculated isosteric heats of adsorption (−31 ± 3 kJ mol^{-1} NH_3 associated with the transformation of Cu(cyhdc) to $Cu(NH_3)_4$(cyhdc); −24 ± 3 kJ mol^{-1}, corresponding to the conversion of Cu(cyhdc) to $Cu(NH_3)_2$(cyhdc); and −39 ± 4 kJ mol^{-1} NH_3 corresponding to conversion of $Cu(NH_3)_2$(cyhdc) to $Cu(NH_3)_4$(cyhdc)) indicate that conversion from $Cu(NH_3)_2$(cyhdc) to Cu(cyhdc) is associated with a lower heat of desorption than the conversion from $Cu(NH_3)_4$(cyhdc) to $Cu(NH_3)_2$(cyhdc). On the other hand, our TGA data show that the former transition is associated with a higher desorption temperature (125 °C versus 50 °C; Supplementary Fig. 11). This probably reflects the presence of a large activation barrier associated with the considerable structural rearrangement that occurs upon transitioning from $Cu(NH_3)_2$(cyhdc) to Cu(cyhdc).

Kinetics of NH_3 adsorption in Cu(cyhdc) and volume changes upon NH_3 uptake

Kinetic data were collected using a Micromeritics ASAP 3Flex volumetric analyser. A glass tube containing 38.6 mg of activated Cu(cyhdc) (activated as described in 'Synthesis of Cu(cyhdc)') was dosed with 1.54 mmol NH_3. The temperature of the sample was controlled using a Syltherm bath held at 25 °C by a water recirculator. The temperature at

the outer surface of the tube was monitored throughout the experiment with a K-type thermocouple. The pressure decay was recorded as a function of time using a sampling frequency of 2 Hz, and the uptake of NH_3 was calculated from mass balance. The resulting data are presented in Supplementary Fig. 30. This preliminary kinetics analysis indicates that NH_3 adsorption in Cu(cyhdc) is rapid, with an estimated time to reach half capacity of less than 40 s at 298 K and 1 bar NH_3. By contrast, metal halides must be dispersed in a porous support (for example, silica and zeolites) to achieve sufficiently rapid adsorption kinetics and stability over many uptake–release cycles, as well as to remedy issues related to the large volume expansion of these materials upon NH_3 adsorption (up to 400%)[8,40]. Using the unit-cell parameters for $Cu(NH_3)_4$(cyhdc) given in Supplementary Table 1 and those for Cu(cyhdc) given in ref. [18], we determined that the framework-to-polymer transition triggered by NH_3 uptake in Cu(cyhdc) is associated with just a 20% volume expansion.

High-pressure NH_3 adsorption measurements

Ultrahigh-purity-grade NH_3 (99.999%, Praxair) was used for all experiments. Activated Cu(cyhdc) (about 130–180 mg) was transferred into a high-pressure sample holder with an isolation valve in an N_2 filled glovebox. A stainless-steel dowel was placed in the holder to minimize the dead space. High-pressure NH_3 isotherms (up to 6 bar) were measured in a walk-in fume hood using an HPVA II-200 high-pressure volumetric analyser from Micrometrics. Isotherms were collected by dosing NH_3 to the sample in a stepwise fashion, and each data point was taken after sufficient time for equilibration (typically 2–4 h for steep uptake regions). The equilibration of each data point was assessed manually, and as a result of the lengthy experimental times (on the order of four to six days), select data points were left to equilibrate for longer periods (for example, overnight), leading to small spurious jumps in the plateau region below 2 bar in Fig. 4d–f. The sample holder temperature was controlled using either a sand bath (373–458 K) or Julabo ME circulator filled with water/ethylene glycol (298 K). For all isotherms, free space corrections were carried out at ambient and analysis temperature using ultrahigh-purity helium gas (99.999%, Praxair).

Preliminary evaluation of Cu(cyhdc) stability following NH_3 adsorption at high temperatures and pressures

As discussed in the main text, NH_3 adsorption data obtained for Cu(cyhdc) at temperatures of 423 K and above and pressures up to 6 bar suggest the formation of a solid with 2 NH_3 bound per Cu site. Direct characterization of this species in situ was not possible with our experimental set-up. However, by way of a preliminary analysis of the stability and reversibility of NH_3 adsorption at higher temperatures and pressures, we exposed a sample of Cu(cyhdc) to 6 bar NH_3 at 423 K for 10 min and analysed the powder diffraction pattern of a portion of the solid (1) after reducing the temperature to 298 K and depressurizing the NH_3 to atmospheric pressure and (2) after subsequently removing NH_3 with heating at 433 K under dynamic vacuum for 18 h using the degas port of an ASAP 2020HD gas adsorption analyser. We also carried out the same manipulations for a sample initially exposed to 6 bar NH_3 for 3 h at 458 K. After cooling and depressurization, samples containing adsorbed NH_3 were handled quickly to minimize exposure time to ambient atmosphere (see 'Preparation and handling of $Cu(NH_3)_4$(cyhdc) prepared from Cu(cyhdc) via dosing with NH_3 gas'). After each manipulation, a portion of the resulting solid was characterized using ex situ powder X-ray diffraction analysis. Data were collected from sealed capillaries packed to the same height (10 mm) with powder, enabling semi-quantitative analysis of peak intensities.

For the sample heated at 423 K under 6 bar NH_3, the ex situ powder X-ray diffraction pattern collected after cooling to room temperature and depressurization features peaks corresponding to $Cu(NH_3)_4$(cyhdc) as well as new sharp reflections due to an unidentified phase (or phases, hereafter, 'component a'; Supplementary Fig. 31). Powder X-ray diffraction data collected upon subsequent desorption of NH_3 at 433 K under dynamic vacuum feature reflections due to Cu(cyhdc), indicating that NH_3 adsorption under these conditions is partially reversible (Supplementary Fig. 32). There are also sharp reflections from a second, as-of-yet-unidentified phase (hereafter, 'component b').

Similar results were obtained for the sample initially heated at 458 K under 6 bar NH_3. In particular, the powder pattern collected after cooling to room temperature and depressurization featured peaks assignable to $Cu(NH_3)_4$(cyhdc) and sharp reflections associated with component a, but additional new peaks were also present ('component c'; Supplementary Fig. 31). Following regeneration of this sample at 448 K for 3 h (Supplementary Fig. 32), the powder pattern features peaks associated with Cu(cyhdc) as well as component b, although less of the latter is present in this sample relative to what was present in the sample regenerated after dosing with 6 bar NH_3 at 423 K. It should also be noted that some irreversible browning of the material was observed after the 3 h exposure to 6 bar NH_3 at 458 K, suggesting that some decomposition occurs as a result of exposure to this higher temperature and/or for a longer contact time. No such browning is observed if the parent framework Cu(cyhdc) is heated to 458 K for multiple hours under dynamic vacuum, however.

Finally, in a third manipulation, the regenerated sample resulting from dosing at 423 K and 6 bar NH_3 was then re-dosed with 1 bar NH_3 at room temperature for 10 min. Ex situ powder diffraction analysis of the resulting solid suggests that both Cu(cyhdc) and component b convert to $Cu(NH_3)_4$(cyhdc) under these conditions (Supplementary Fig. 33a). In addition, the infrared spectrum of this same sample (Supplementary Fig. 33b) essentially overlays with that of freshly prepared $Cu(NH_3)_4$(cyhdc). Thus, these preliminary data indicate that, although the mechanism of NH_3 uptake in Cu(cyhdc) at high pressures and temperatures is different (and perhaps more complex) than at room temperature and pressures up to 1 bar, NH_3 can be desorbed and re-adsorbed at least once to generate $Cu(NH_3)_4$(cyhdc) at 1 bar NH_3.

Powder X-ray diffraction

Laboratory powder X-ray diffraction data were collected on a Bruker AXS D8 Advance diffractometer equipped with a Cu Kα source (wavelength 1.54 Å). High-resolution synchrotron X-ray powder diffraction data were collected at beamline 17-BM at the Advanced Photon Source at Argonne National Laboratory with a Perkin-Elmer α-Si flat-panel detector. Diffraction patterns were collected at a wavelength of 0.44850 Å and the sample temperature was held constant at 298 K with an Oxford Cryosystems Cryostream 800. Samples of the activated frameworks (about 5 mg) were loaded into 1.0 mm boron-rich glass capillaries and flame sealed. Activated Cu(cyhdc) was loaded into a capillary in air, and flame sealed within 15 s of exposure to ambient conditions. Air-sensitive Cr(cyhdc) and Fe(cyhdc) were loaded into capillaries inside a dry N_2 glovebox, the capillaries were sealed with grease, and then taken into the air and quickly flame sealed. For NH_3-dosed samples, capillaries were loaded with about 5 mg of activated framework in air or a dry N_2 glovebox and then attached to a gas cell. The gas cell was connected to the analysis port of a Micromeritics ASAP 2020 gas adsorption analyser, evacuated to remove N_2 or air, and then dosed with 1 atm NH_3. Capillaries were then flame sealed with NH_3 in the headspace.

The structure analyses, including indexing and Pawley and Rietveld refinements, were performed with the program TOPAS-Academic v4.1.16. The structure of Fe(cyhdc) was refined using a simulated annealing approach where the asymmetric unit was constructed as a rigid body using *z*-matrix notation. Three degrees of rotation and translation were allowed for the entire rigid body and bond lengths and angles were allowed to refine freely within predefined limits. Atom positions for the Rietveld refinement were extracted from the simulated annealing refinement with the best goodness of fit and further optimized to yield the reported structure (Supplementary Fig. 19). A Pawley refinement was used to obtain unit-cell parameters for Cr(cyhdc) (Supplementary Fig. 20).

Single-crystal X-ray diffraction measurements

X-ray diffraction analysis was performed on single crystals coated with paratone-N oil and mounted on MiTeGen loops. The crystals were frozen at 100(2) K by an Oxford Cryosystems Cryostream 700. Data were collected at the UC Berkeley CHEXRAY crystallographic facility on a Rigaku XtaLAB P200 equipped with a MicroMax 007HF rotating anode and a Pilatus 200K hybrid pixel array detector using Cu Kα radiation (wavelength 1.5418 Å). Data collection, processing and reduction were performed with CrysAlis^{Pro} software[41]. A multi-scan absorption correction was applied using the SCALE3 ABSPACK scaling algorithm within CrysAlis^{Pro}. No crystal decay was observed during data collection. Structures of $Cu(NH_3)_4$(cyhdc), $Cu(NH_3)_2$(cyhdc) and $Cu(NH_3)_2(H_2O)$(cyhdc) were solved by intrinsic phasing with SHELXT[42] and $Cu(H_2O)_2$(tfbdc) was solved using direct methods with SHELXS[43,44]. The structure of $Cu(H_2O)_2$(tfbdc) was solved as a two-component twin [−1 0 0 0 −1 0 0.1288 0.5342 1; BASF = 0.487(2)]. All structures were refined using SHELXL[45] operated in the OLEX2[46] interface. Thermal parameters were refined anisotropically for all non-hydrogen atoms. For $Cu(NH_3)_4$(cyhdc) and $Cu(NH_3)_2$(cyhdc), hydrogen atoms were included at the geometrically calculated positions and refined using a riding model. For $Cu(H_2O)_2$(tfbdc) and $Cu(NH_3)_2(H_2O)$(cyhdc), hydrogen atoms were found in the electron difference map. Crystallographic data are summarized in Supplementary Table 1.

Thermogravimetric analysis

TGA was performed using a TA Instruments Discovery TGA. Decomposition experiments were performed under dry N_2 (flow rate 25 ml min^{-1}) at a ramp rate of 1 °C min^{-1}. For TGA cycling tests, approximately 10 mg of activated Cu(cyhdc) was placed in a tared TGA pan, and dosed with 1 bar NH_3 using a Micromeritics 3Flex gas adsorption analyser. After sitting for 30 min under an atmosphere of pure NH_3, the TGA pan was then quickly transferred to the TGA instrument. It is noted that as discussed above, $Cu(NH_3)_4$(cyhdc) prepared by gas dosing in this way is sensitive to ambient atmosphere and will lose NH_3 and adsorb atmospheric H_2O (Supplementary Fig. 29). A sample of $Cu(NH_3)_4$(cyhdc) held in a TGA pan will retain its blue colour and phase purity via powder X-ray diffraction analysis (Supplementary Fig. 34b) provided it is not exposed to air for more than about 60 s, whereas a thin layer of $Cu(NH_3)_4$(cyhdc) spread out on a flat surface will change colour much more rapidly, with some colour change evident after 1 min (Supplementary Fig. 29). In the TGA instrument, the sample of $Cu(NH_3)_4$(cyhdc) was heated to 160 °C at a rate of 1 °C min^{-1} and then held isothermally for 60 min, all under a flow of N_2 (25 ml min^{-1}), to desorb all NH_3. The temperature was then ramped down to a final temperature of 25 °C at 5 °C min^{-1}. This adsorption–desorption procedure was repeated six times on the same sample (Supplementary Fig. 12). After the sixth cycle, a portion of the material was placed in a glass capillary and dosed a seventh time with NH_3. The powder X-ray diffraction pattern of the resulting solid is shown in Supplementary Fig. 13 and overlays with the pattern obtained upon initial dosing with NH_3.

Adsorption of NH_3 under humid conditions

At short exposure times of about 12 min, Cu(cyhdc) adsorbs NH_3 selectively in the presence of humidity to form $Cu(NH_3)_4$(cyhdc) (Supplementary Fig. 34). However, we note that even at this short contact time, weak reflections from a new phase can be identified in the powder X-ray diffraction pattern of the resulting solid (Supplementary Fig. 35). These reflections are not assignable to $Cu(NH_3)_4$(cyhdc), Cu(cyhdc) or $Cu(NH_3)_2(H_2O)$(cyhdc). Even still, the infrared spectroscopy data presented in Supplementary Fig. 34a suggest that H_2O co-adsorption is minimal under these conditions. Cycling experiments were performed as follows. A sample of Cu(cyhdc) (about 10 mg) was loaded into a TGA pan and placed in a 20 ml vial containing an open 1.8 ml vial loaded with 1 ml of about 28% aqueous NH_3. The larger vial was sealed, and the sample was left undisturbed for 12 min, after which it was rapidly transferred to the TGA instrument for analysis (as described above for dry dosing experiments). Under these conditions, the material is stable to several humid NH_3 adsorption and desorption cycles (Supplementary Fig. 36).

If Cu(cyhdc) is exposed to humid NH_3 for 20 min, the powder diffraction pattern of the resulting solid is distinct from that of $Cu(NH_3)_4$(cyhdc), suggesting a new crystalline phase results from the reaction of H_2O vapour with $Cu(NH_3)_4$(cyhdc) in the presence of NH_3 (Supplementary Fig. 35). This new phase does not form when Cu(cyhdc) is exposed to H_2O vapour or NH_3 alone (Supplementary Fig. 37). We note that the blue colour and powder X-ray diffraction pattern of this phase are distinct from $Cu(NH_3)_2(H_2O)$(cyhdc) (see above and Supplementary Fig. 29).

To further probe the co-adsorption of H_2O during humid NH_3 exposure, a time-course experiment was performed in which four samples of Cu(cyhdc) (5 mg) were placed in open 4 ml vials, heated at 150 °C briefly under dynamic vacuum on a Schlenk line, refilled with N_2, quickly capped and allowed to cool to room temperature. Separately, a 100 ml jar was charged with 10 ml of about 28% aqueous NH_3, and the atmosphere inside the jar was allowed to equilibrate for 30 min. After this equilibration, the four samples were placed into the jar, which was then quickly sealed. A vial was removed from the jar at pre-determined times (after 4 min, 8 min, 12 min and 20 min), a portion of the solid from the vial was quickly loaded into a glass capillary under air, and the capillary sealed for analysis by powder X-ray diffraction (Supplementary Fig. 35). The resulting data suggest selectivity for NH_3 over H_2O is achieved at short contact times, despite a small amount of H_2O co-adsorption.

DFT estimation of hydrogen-bonding contribution to NH_3 adsorption

Starting from the crystallographic coordinates of $Cu(NH_3)_4$(cyhdc), periodic DFT calculations were performed using the BP86 functional. The 6-311++G** basis set was used for all hydrogen and oxygen atoms. The 6-311G* basis set was used for all other atoms. The positions of the hydrogen atoms were geometry optimized, and all other atoms and the unit cell were frozen. The coordinates of this model are reported in Supplementary Table 2. The polymer chains were then artificially separated by doubling the lengths of the first and third translation vectors reported in Supplementary Table 2, and the hydrogen-atom positions were allowed to relax. The difference between the electronic energies of these models is $\Delta E = -45.0$ kJ mol^{-1} NH_3, and this value represents an estimate of interchain hydrogen-bonding energy.

DFT models of Cu(bpdc) and Cu(tfbdc)

Starting from the crystallographic coordinates of Cu(bdc)[47], the hydrogen atoms were replaced with fluorine atoms to generate a starting structure for Cu(tfbdc). Similarly, the bdc^{2-} linkers in the Cu(bdc) structure were replaced with (planar) $bpdc^{2-}$ linkers to generate a starting structure for Cu(bpdc). Geometry optimizations were then carried out at the BP86/6-311G* level. The coordinates of the optimized models are reported in Supplementary Tables 3 and 4.

Data availability

Crystal structure data are available in the Cambridge Structural Database under deposition numbers 2202925, 2203378, 2203379, 2203380 and 2208967. All other data are available from the corresponding author upon request.

39. Frisch, M. J. et al. *Gaussian 16, Revision A.03* (Gaussian, 2016).
40. Jiang, L. & Roskilly, A. P. Thermal conductivity, permeability and reaction characteristic enhancement of ammonia solid sorbents: a review. *Int. J. Heat Mass Transf.* **130**, 1206–1225 (2019).
41. *Rigaku Oxford Diffraction CrysAlis^{Pro} Software System*, version 1.171.39.7a (Rigaku, 2015).

42. Sheldrick, G. M. Crystal Structure Refinement with SHELXL. *Acta Crystallogr. C* **71**, 3–8 (2015).
43. Sheldrick, G. M. *SHELXS* (Univ. Göttingen, 2014).
44. Sheldrick, G. M. A short history of SHELX. *Acta Crystallogr. A* **64**, 112–122 (2008).
45. Sheldrick, G. M. *SHELXL* (Univ. Göttingen, 2014).
46. Dolomanov, O. V., Bourhis, L. J., Gildea, R. J., Howard, J. A. K. & Puschmann, H. OLEX2: a complete structure solution, refinement and analysis program. *J. Appl. Crystallogr*. **42**, 339–341 (2009).
47. Carson, C. et al. Structure solution from powder diffraction of copper 1,4-benzenedicarboxylate. *Eur. J. Inorg. Chem*. **2014**, 2140–2145 (2014).

Acknowledgements This research was supported by the US Department of Energy, Office of Basic Energy Sciences, Separation Science in the Chemical Sciences, Geosciences, and Biosciences Division, under Award Number DE-SC0019992. We are grateful for the support of BERS through an Arnold O. Beckman Postdoctoral Fellowship in Chemical Sciences and of ABT and EOV through NSF Graduate Research Fellowships (DGE 1752814). DFT calculations were performed using infrastructure from the UC Berkeley Molecular Graphics and Computation Facility, which is supported by the NIH (NIH S10OD023532). Use of the APS at Argonne National Laboratory was supported by US Department of Energy, Office of Science, Office of Basic Energy Sciences, under Contract no. DE-AC02-06CH11357. We acknowledge K. R. Meihaus for editorial assistance.

Author contributions B.E.R.S. and J.R.L. designed the research. B.E.R.S., A.B.T., H.F., E.O.V., M.V.P. and M.N.D. performed the experiments. B.E.R.S. and J.R.L. analysed the data. B.E.R.S. wrote the manuscript. B.E.R.S. and J.R.L. edited the manuscript.

Competing interests The authors declare no competing interests.

Additional information

Supplementary information The online version contains supplementary material available at https://doi.org/10.1038/s41586-022-05409-2.

Correspondence and requests for materials should be addressed to Jeffrey R. Long.

Peer review information *Nature* thanks Hiroshi Kitagawa and the other, anonymous, reviewer(s) for their contribution to the peer review of this work.